


Monitoring Mouse Surface Temperature During Stress with a Thermal Camera: A Low-Cost Infrared Videography System for Evaluating Murine Metabolism

Breanna Page,^{1,2} Carolina Cora,^{1,3} James Reilly,¹ Ryan Reno,¹ Wadak Harbi,¹ Maureen S. Lynes,⁴ Michael A. Lynes,⁵ and Matthew D. Lynes^{1,2,3,6,7} 

¹Center for Molecular Medicine, MaineHealth Institute for Research, Scarborough, Maine

²Roux Institute at Northeastern University, Portland, Maine

³Graduate School of Biomedical Science and Engineering, University of Maine, Orono, Maine

⁴Accent Therapeutics, Lexington, Massachusetts

⁵Department of Molecular and Cell Biology, University of Connecticut, Storrs, Connecticut

⁶Department of Medicine, MaineHealth, Portland, Maine

⁷Corresponding author: matthew.lynes@mainehealth.org

Published in the Toxicology section

Energy is required for life, and organisms obtain their energy from fuel sources to enable both anabolic and catabolic processes. Some of this energy is radiated as heat, which can be quantified as a measure of metabolic rate. In some cases, environmental toxicants can alter metabolic energy in undesirable ways, and characterization of new pharmaceuticals can determine the efficacy of desirable metabolic rate manipulation or identify off-target adverse effects. Current methods to directly measure heat production in laboratory mice are expensive, can be laborious, and make it challenging to monitor animals in ways that are multiplexed, robust, and non-invasive. We present a set of protocols for assembling and deploying a simple, low-cost thermal camera to monitor and record thermogenic activity, modified from prior work. Parts used to build this system currently cost approximately \$150 USD and, when assembled, can record mouse temperatures as well as ambient cage temperatures up to twice per second for extended periods. By using multiplexed cameras in a diurnal mouse incubator system, the thermogenic capacity of several mice can be simultaneously recorded and graphed. Exogenous agents and genotypes that alter metabolism can be readily identified with this technology. In this set of protocols, we describe the assembly of the thermal video camera device, its use, and related data capture and analysis methods. © 2025 The Author(s). Current Protocols published by Wiley Periodicals LLC.

Basic Protocol 1: Assembling thermal camera for thermogenic stress test

Basic Protocol 2: *In vivo* measurement of mouse temperature under different ambient conditions

Keywords: brown adipose tissue • infrared camera • metabolism • thermal output • thermogenesis

If you found this article helpful, please cite it.

How to cite this article:

Page, B., Cora, C., Reilly, J., Reno, R., Harbi, W., Lynes, M. S.,
Lynes, M. A., & Lynes, M. D. (2025). Monitoring mouse surface
temperature during stress with a thermal camera: A low-cost
infrared videography system for evaluating murine metabolism.
Current Protocols, 5, e70098. doi: 10.1002/cpz1.70098

INTRODUCTION

An organism's metabolic activity is the sum of a complex set of chemical reactions that sustain life, growth, and reproduction. These processes involve the breakdown of nutrients (catabolism) to release energy and the synthesis of essential biomolecules (anabolism) for all cellular functioning. The measurement of an organism's metabolic activity provides information crucial to a variety of fields of study, including toxicology, physiology, nutrition, and pharmacology, as it yields insights into overall health, energy expenditures, and the responses that an organism can make to changes in its external environment or to pharmacologic interventions. An organism's level of metabolic activity is known to exhibit regular patterns that are influenced by circadian rhythms and other biological cycles. These circadian rhythms are endogenous, self-sustaining oscillations that occur approximately every 24 hr and are known to regulate a variety of physiological processes, including sleep-wake cycles, hormone secretion, and basal metabolic activity. These rhythms are driven by an internal biological clock and themselves can be influenced by external cues, such as light and temperature. In addition to circadian rhythms, metabolic activity can also be influenced by other rhythms, such as ultradian rhythms (shorter cycles within a 24-hr period) and infradian rhythms (longer cycles spanning days or weeks) (Coskun et al., 2023). These rhythms can also vary and are affected by factors such as feeding patterns, physical activity, and environmental conditions. When making measurements of metabolic activity, it is essential to be mindful of these rhythms in designing the time points at which measurements are made.

Each organ system within the body consumes energy to perform work, and as a result of these metabolic processes, heat is released as a byproduct. In addition to the obligatory energy expenditure required for life, voluntary energy expenditure is derived from all activities that are modifiable, including heat produced in response to environmental challenges in a process called adaptive thermogenesis (Chouchani et al., 2019; Tseng et al., 2010). Changes in heat production and energy expenditure can be both the product and the result of pathophysiology. For example, obesity can decrease heat production and energy expenditure per unit of body weight, whereas increasing these catabolic processes can promote weight loss. There are also natural rhythms of body temperature, including an overall drop in temperature during the rest period as well as ultradian pulses of heat that occur in mice and humans approximately hourly (Blessing, 2018; Ootsuka et al., 2009; Shimatani et al., 2021). In mice, these pulses of heat occur more often in males than females, and they can be altered by pregnancy (Kuroyanagi et al., 2022; Smarr & Kriegsfeld, 2022). Whether alterations to the ultradian rhythms of thermogenesis can underlie pathophysiological conditions is unknown.

Given the complexity of directly measuring metabolic activity, scientists often rely on surrogate measures. One such measure is body temperature, which is frequently used as a proxy for metabolic activity because many metabolic processes generate heat as a byproduct. As metabolic activity increases, more energy is released, leading to an increase in body temperature. Conversely, a decrease in metabolic activity can result in

a lower body temperature. Rapid and regular measurements of temperature can provide valuable insights into metabolic activity and its fluctuations over time (Madhvapathy et al., 2024). It is important to note that the relationship between metabolic activity and temperature can vary across different species. Factors such as body size, insulation (e.g., fur or feathers), and other evolutionary adaptations can influence the magnitude and distribution of thermal signals associated with metabolic activity. For example, small mammals with a high surface-area-to-volume ratio tend to have higher metabolic rates and may exhibit more pronounced thermal signals compared to larger mammals. Similarly, species adapted to cold environments may have enhanced thermogenic (heat production) mechanisms, such as increased brown fat activity, to maintain body temperature in those colder conditions.

Brown adipose tissue (BAT), also known as brown fat, is a specialized tissue that plays a crucial role in thermogenesis and energy expenditure (Frontini & Cinti, 2010). Unlike white adipose tissue, which primarily stores energy, brown fat is rich in mitochondria and specialized proteins that enable the release of chemical energy as heat. BAT distribution varies across different age groups in humans (Cypess et al., 2009). In infants, BAT is primarily found in the neck, back, and shoulders (Lidell et al., 2013). As individuals progress through adolescence, BAT becomes more widely distributed throughout the body. In adult humans, BAT is concentrated around the neck, adrenal glands, heart, chest, and kidneys (Cypess et al., 2013; Sacks & Symonds, 2013). In mice, BAT is found in anterior subcutaneous depots (deep cervical, superficial cervical, interscapular, subscapular, and axillo-thoracic) and in posterior subcutaneous depots (dorso-lumbar, inguinal, and gluteal) as well as in several visceral depots (mediastinal, mesenteric, retroperitoneal, and abdominopelvic) (Mo et al., 2017). Despite these distinctions in BAT distribution, the two species show similar responses to cold exposure, with increased glucose uptake and activation of BAT.

The experimental measurement of energy expenditure falls into many different technical approach categories (Table 1). Each of these methods has advantages and disadvantages. Historically, the most commonly used measure has been indirect calorimetry, which quantifies oxygen consumption and carbon dioxide production using a metabolic cage (Rubio et al., 2023). As the method's name implies, indirect measurements can be used to approximate metabolic heat production, but they can underestimate the actual resting metabolic rate. Indirect calorimetry measurements using metabolic cages can be time-consuming to set up and operate, and this approach may not capture the dynamic changes in metabolic activity that occur throughout the day or in response to specific stimuli. Here, we describe the assembly (Basic Protocol 1) and implementation (Basic Protocol 2) of a low-cost infrared camera system to monitor mouse energy expenditure in real time.

Direct calorimetry, in contrast, is used to measure energy expenditure in sequestered organisms over short periods (minutes to days). Maximizing the sensitivity of direct calorimetry is technically challenging because the test subject must be enclosed in an insulated chamber to measure heat production. These chambers are expensive to build and operate and consequently are infrequently employed.

Surgically implanted wireless temperature and motility detectors can also be used to continuously monitor temperature and physical activity and provide a different option for evaluating metabolic activity and its relationship with temperature and movement. Although more convenient than metabolic cage measurements, implantable temperature loggers can themselves influence thermal measurements by inducing acute and chronic inflammatory responses at the implanted probe site, which alter baseline temperatures (Madhvapathy et al., 2024).

Table 1 Comparison of Approaches to Measure Mouse Thermogenesis

Approach	Pros	Cons
Metabolic cages	<ul style="list-style-type: none">• Direct measurement of gas exchange provides accurate estimates of metabolic rate.• Allows for the study of metabolic responses to various interventions or environmental conditions.• Can be used for both small and large animals.	<ul style="list-style-type: none">• Requires specialized equipment and controlled environmental conditions.• Confines the animal’s movement, which may affect natural behavior and metabolic activity.• Measurements are typically taken over a limited time period, potentially missing dynamic changes in metabolic activity.
Surgically implanted temperature and motility detectors	<ul style="list-style-type: none">• Allows for continuous, long-term monitoring of temperature and motility.• Provides data on the dynamic changes in metabolic activity over time.• Can be used in free-moving animals, minimizing the impact on natural behavior.	<ul style="list-style-type: none">• Requires invasive surgical procedures, which can be stressful for the animal and introduce potential complications.• Implanted devices may have limited battery life or signal range, requiring periodic replacement or maintenance.• Data analysis and interpretation can be complex, especially when correlating temperature and motility with metabolic activity.
FDG PET/CT fusion imaging	<ul style="list-style-type: none">• Non-invasive and provides detailed anatomical and functional information.• Allows for the localization and quantification of metabolic activity in specific tissues or organs.• Can be used to study metabolic responses to interventions or disease states.	<ul style="list-style-type: none">• Involves exposure to ionizing radiation, which may limit its use in certain populations or research settings.• Requires specialized equipment and trained personnel, making it relatively expensive and less accessible.• Provides a snapshot of metabolic activity at a specific time point, potentially missing dynamic changes over time.

Another method for quantifying energy expenditure, the doubly labeled water (DLW) method, in which water is labeled with non-radioactive isotopes of each element (deuterium, ²H, and oxygen-18, ¹⁸O), can be used to estimate energy expenditure in organisms over longer periods (e.g., >1 week) with similar accuracy to calorimetric approaches (Roberts et al., 1986). However, this method lacks resolution over shorter periods.

A final category of strategies for quantifying energy expenditure in organisms relies on a variety of technical approaches to collect images of the experimental subject, from which metabolic data can be extracted. Positron emission tomography (PET) is an imaging approach that can evaluate the uptake of radiolabeled metabolic substrates such as glucose into specific tissues (Virtanen, 2016). Radioactive F-fluorodeoxyglucose (FDG) is administered, and PET, combined with computed tomography (CT; together called “FDG PET/CT”), can follow the localization of the radioactive signal and the tissues in which it accumulates over time as an indication of metabolic activity. This technology has clinically important applications to localize metabolically active cancer tissue and to determine the cancer’s response to therapy.

Similarly, magnetic resonance imaging (MRI) can be used to quantify proton density in fat tissue, which can change when thermogenesis is activated (Holstila et al., 2017). This imaging modality has drawbacks, such as the high cost of the imaging technology, a practical limit to the ability to observe changes over extended timeframes, and the use of ionizing radiation, with its associated complex regulatory and practical challenges.

Thermal imaging, also known as infrared thermography (IRT), has become valuable as a simpler and more versatile imaging approach to studies of metabolic activity. Thermal imaging techniques can localize the thermal signal to specific regions of the body, such

as the interscapular region, where brown fat deposits are typically found in many mammalian species. This localization of the thermal signal to brown fat can provide valuable insights into the activation and function of this tissue within the context of the overall metabolic activity of the organism. IRT can be used both for studies of body movement and for metabolic activity assessments and is readily used over both brief and longer timespans with little if any consequence to the observed subject. Thermal imagers, such as forward-looking infrared (FLIR) cameras, can detect and visualize the infrared radiation emitted by objects, allowing for the measurement of surface temperatures without direct contact with the subject.

Beyond body movement studies, FLIR images can provide valuable information in various other contexts. In particular, thermal imaging techniques can provide both average temperature and minimum/maximum body temperature measurements. Extracting the average temperature across the body can be useful for assessing overall metabolic activity and for detecting subtle changes in temperature distribution across the body. Time-stamped measurements collected over extended periods can inform the understanding of circadian, ultradian, and infradian rhythms in metabolic activity. This thermal imaging approach can be particularly valuable when studying whole-body thermogenesis or investigating the effects of pharmacologic interventions or changing environmental conditions on overall energy expenditure. Thermal imaging can also be used to monitor physiological processes like blood flow (Bagavathiappan et al., 2009), inflammation (Ramirez-GarciaLuna et al., 2022), and wound healing (Monshipouri et al., 2021) by detecting temperature changes in specific regions of the body. In some cases, focusing on the maximum body temperature may be the most informative, especially when studying localized thermal signals associated with specific anatomical regions of interest, such as brown fat deposits. The maximum temperature can provide insights into the activation and function of these tissues, which may not be as apparent when considering the average temperature across the entire body. The choice between using average or maximum body temperature measurements depends on the specific research objectives, the target tissue or organ of interest, and the experimental design. In some cases, a combination of both approaches (i.e., whole-body and tissue-specific) may be beneficial to gain a comprehensive understanding of metabolic activity and its thermal manifestations.

Overall, the use of thermal imaging and FLIR cameras offers a non-invasive and versatile approach to studying various aspects of physiology, behavior, and environmental interactions, making it a valuable tool in a wide range of research and practical applications. Most commercially available FLIR systems have a form factor that is not compatible with *in situ* measures of body temperature of small animals in animal care settings, tend to be costly, and are not formatted for easy multiplexing in an experimental context. The instrumentation and protocols provided here are designed to address those shortcomings.

NOTE: All protocols involving animals must be reviewed and approved by the appropriate Animal Care and Use Committee and must follow regulations for the care and use of laboratory animals.

ASSEMBLING THERMAL CAMERA FOR THERMOGENIC STRESS TEST

These instructions for assembling the thermal camera imager describe the use of an inexpensive and readily available Raspberry Pi 4 single-board computer as part of a low-cost infrared videography system (Hrisko, 2020). The Raspberry Pi 4 computer has built-in I2C interfaces and native I2C hardware support, making it the best choice compared to computers like a Mac or PC that lack support for low-level hardware interfacing. Assembly should take ~20 min. The specialty parts for this system were obtained from Adafruit (<https://www.adafruit.com>), but there are other suppliers of equivalent parts. The system described should cost approximately \$150 USD in total at current prices, is compatible

BASIC PROTOCOL 1

Page et al.

5 of 19

with multiplexed simultaneous recordings of multiple animals, and simplifies placement of the small thermal camera itself within typical mouse cages, which is more challenging with commercial IRT imaging systems that have a larger form factor. Moreover, the system facilitates rapid ongoing automated recordings that minimize disturbances to the experimental animals.

Materials

Raspberry Pi 4 Model B - 4 GB RAM (Adafruit, product ID: 4296) (“Raspberry Pi”)
EVO Plus microSDXC Memory Card 64 GB (Samsung, SKU: MB-MC64H/MB-MC64HA/AM) (“memory card”)
CanaKit Raspberry Pi 4 Case - Premium White (High-Gloss) (CanaKit, SKU: RSP-CASE4-PI4-WHT) (“case”)
Premium Female/Female Jumper Wires - 20 × 3” (75 mm) (Adafruit, product ID: 1951) (“jumper wires”)
STEMMA QT / Qwiic JST SH 4-pin to Premium Male Headers Cable - 150 mm Long (Adafruit, product ID: 4209) (“header cable”)
Adafruit MLX90640 24 × 32 IR Thermal Camera Breakout - 110 Degree FoV (Adafruit, product ID: 4469) (“thermal camera”)
Perma-Proto Half-sized Breadboard printed circuit board – Single (Adafruit, product ID: 1609) (“PCB”)
Electronics-Salon Metric M2.5 Hex Male-Female Brass Standoff (Electronics-Salon, product ID: SP-CTZ2.5) (“standoff”)
CanaKit Raspberry Pi 4 PiSwitch (USB-C) (CanaKit, SKU: RSP-PISWITCH-USBC) (“switch”)
CanaKit 3.5A Raspberry Pi 4 Power Supply (USB-C) (CanaKit, SKU: DCAR-RSP-3A5-C) (“power supply”)
Mini Wireless Keyboard X1 With Touchpad Mouse + LED Backlit (Adafruit, product ID: 922) (“keyboard”)
Micro HDMI to HDMI Cable (Adafruit, product ID: 922) (“HDMI cable”)
10.1-in. LCD Raspberry Pi 4 Model B Touch Screen 1024 × 600 Capacitive Touch Display for Raspberry Pi 4B/3B+/3B PC Jetson Nano (ROADOM, product ID: B09XDK2FRR) (“touch screen”)
USB-A to Micro-USB Cable (Adafruit, product ID: 2185) (“USB cable”)

NOTE: Connections between the electrical components are press-fit and do not require tools. It may be helpful to have a small flat screwdriver and small needle-nose pliers to facilitate making some connections.

1. Organize all of the components as shown in Figures 1 and 2.
2. Orient the Raspberry Pi as shown in Figure 3A and then flip it upside down and insert the memory card into the micro memory card slot (Fig. 3B).
3. Place Raspberry Pi in the case (Fig. 4).

Figure 4B shows the pins to which jumper cables will subsequently be attached (see step 4).

4. Connect four jumper wires to the general-purpose input/output (GPIO) pins (Fig. 5A). Connect a red wire to the first bottom-row pin, a black wire to the third pin in the top row, a blue wire to the second pin in the bottom row (adjacent to the red wire), and a green wire to the third pin in the bottom row (next to the blue wire) (Fig. 5B).
5. Connect the header cable to the thermal camera (Fig. 6A). To do this, connect the other ends of each of the four wires from step 4 to the corresponding color of the header cable (Fig. 6B). Connect red to red, black to black, blue to blue, and green to yellow (Fig. 6C).



Figure 1 Component organization. All necessary components for the thermal camera assembly are laid out and identified, including the Raspberry Pi, case, thermal camera, cables, PCB, and peripherals.

6. Screw the thermal camera into the PCB by hand using a standoff (Fig. 7).
7. Connect the switch to the power supply (Fig. 8A). Plug the switch into the USB connector on the Raspberry Pi. Plug the power supply into a 120-V power source.
If done correctly, a red LED will illuminate on the Raspberry Pi (Fig. 8B).
8. Remove the USB wireless dongle from the back of the keyboard (Fig. 9A) and connect to available USB connector on the Raspberry Pi (Fig. 9B).
The keyboard is powered by a battery (Fig. 9A and step 10).
9. Plug the larger end of the HDMI cable into the HD “IN” connector on the back of the touch screen (Fig. 10A). Connect the micro HDMI end of this cable to the Raspberry Pi micro HDMI connector (Fig. 10B).
10. Plug the USB cable into the power connector on the back of the touch screen (Fig. 11A). Connect the USB-A end of the cord to a power supply (Fig. 11B)
If connected properly, the screen will turn on (Fig. 11C).
11. Install the latest version of the Raspian operating system on the Raspberry Pi.
Follow the instructions from <https://www.raspbian.org/RaspbianInstaller>.

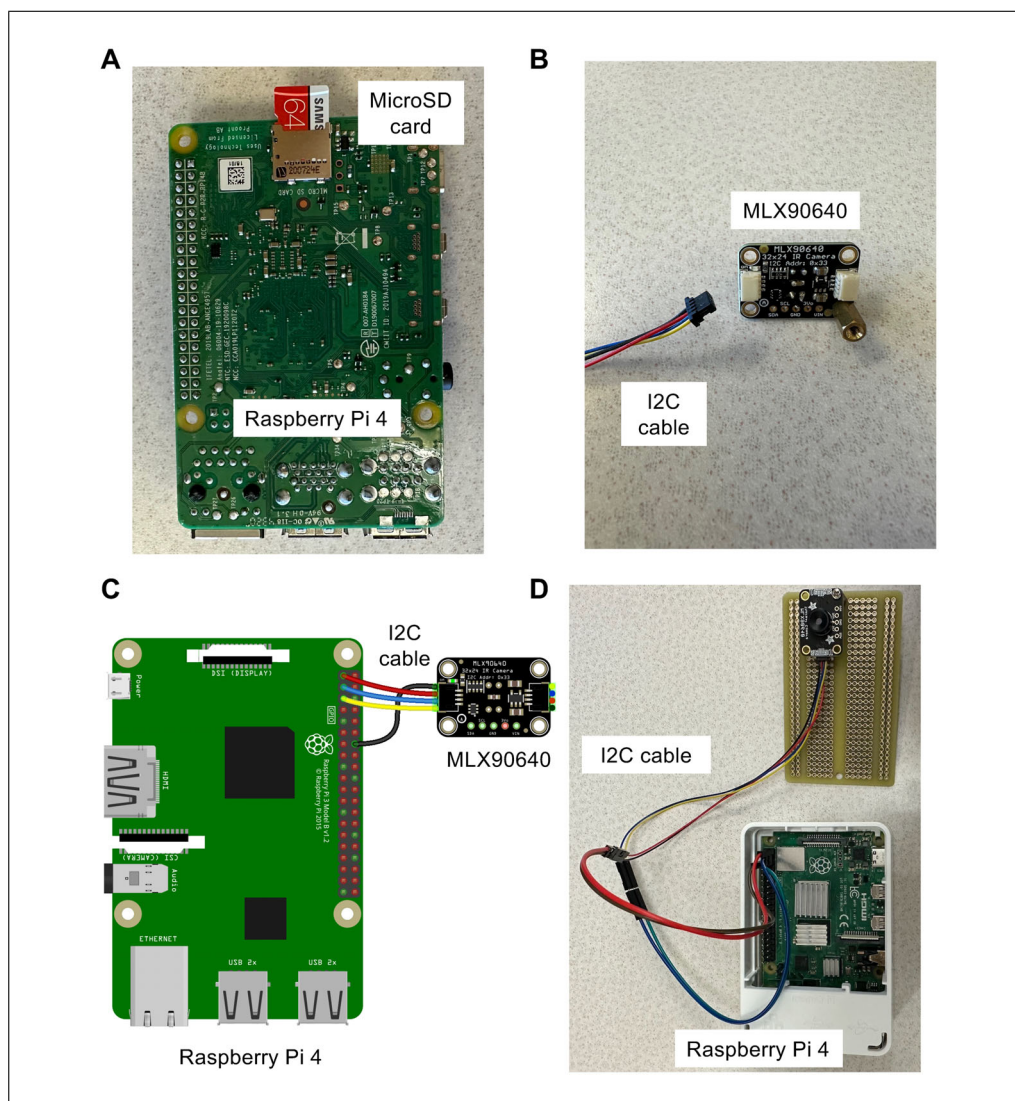


Figure 2 Components and assembly of the thermal imaging system. (A) Raspberry Pi 4, MicroSD card, MLX90640 thermal camera, and I2C cable. (B) Raspberry Pi 4 connected to the MLX90640 thermal camera via the I2C cable. (C) Fully assembled thermal imaging system with all components connected. (D) Connection between the Raspberry Pi 4 and the MLX90640 on the breadboard to the thermal camera using the I2C cable.

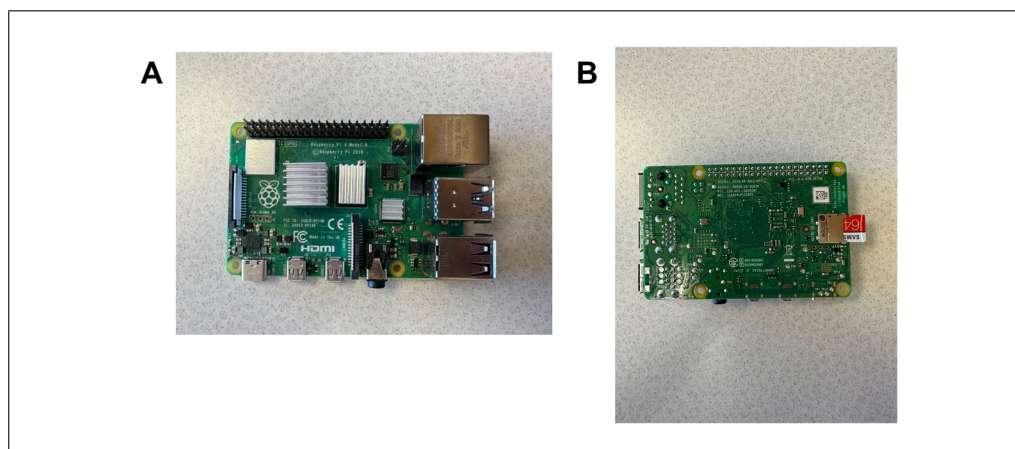


Figure 3 Raspberry Pi preparation. Raspberry Pi 4 Model B (4 GB RAM) before (A) and after (B) the Samsung EVO Plus 64 GB microSDXC memory card being inserted into the micro memory card slot.

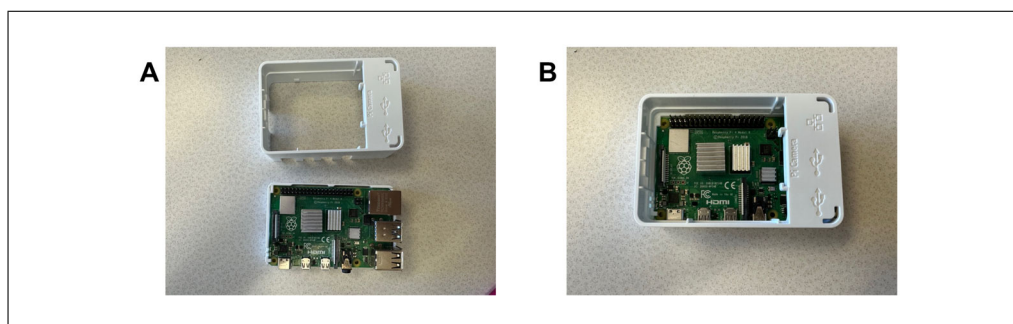


Figure 4 Protective case installation. (A) Raspberry Pi 4 Model B with case and (B) Raspberry Pi placed securely within the CanaKit Raspberry Pi 4 case for protection.

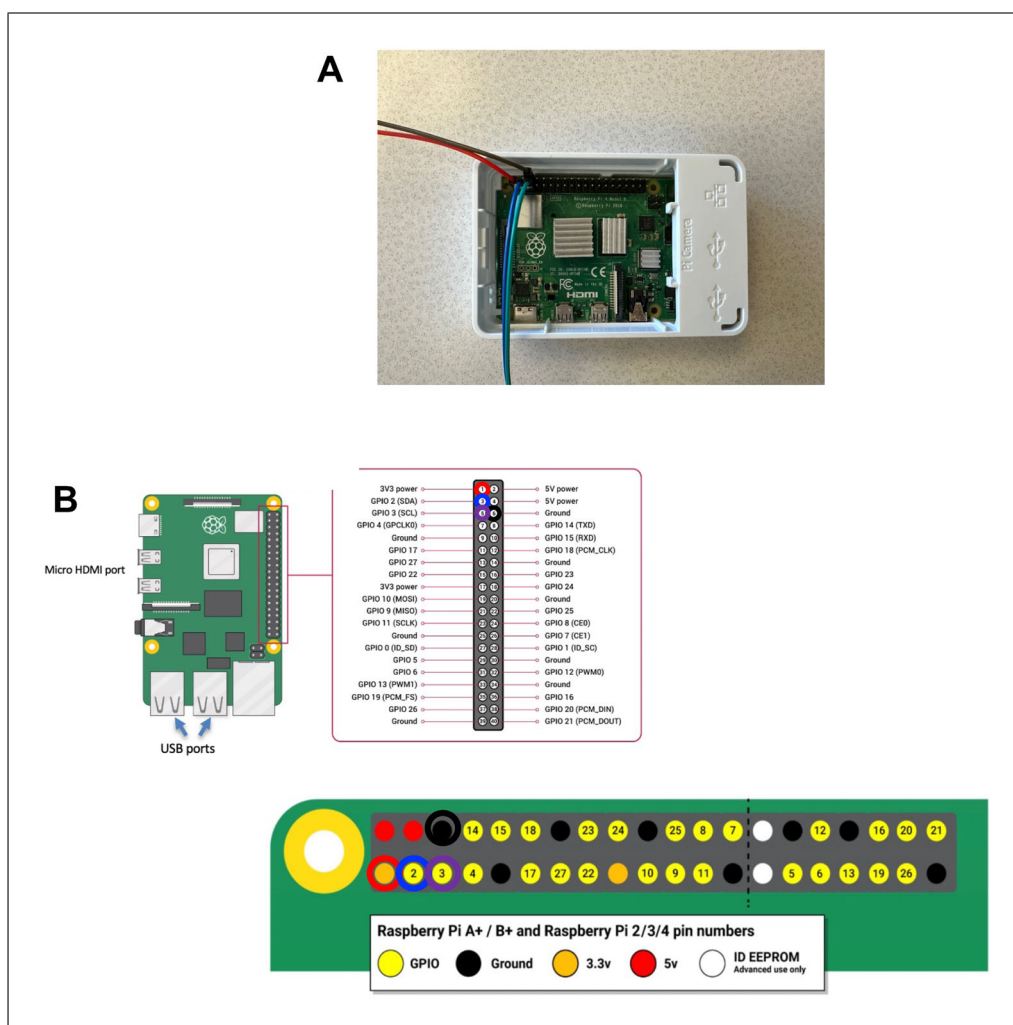


Figure 5 Jumper cable connection. (A) Four female/female jumper wires connected to specific GPIO pins on the Raspberry Pi. (B) Pin identifications for the Raspberry Pi showing pins for 3.3 V (red), ground (black), SDA (blue), and SCL (purple).

12. Open the terminal application on the touch screen and install the appropriate libraries by entering the following commands:
 - “sudo pip3 install matplotlib scipy numpy”
 - “sudo apt-get install -y python-smbus”
 - “sudo apt-get install -y i2c-tools”

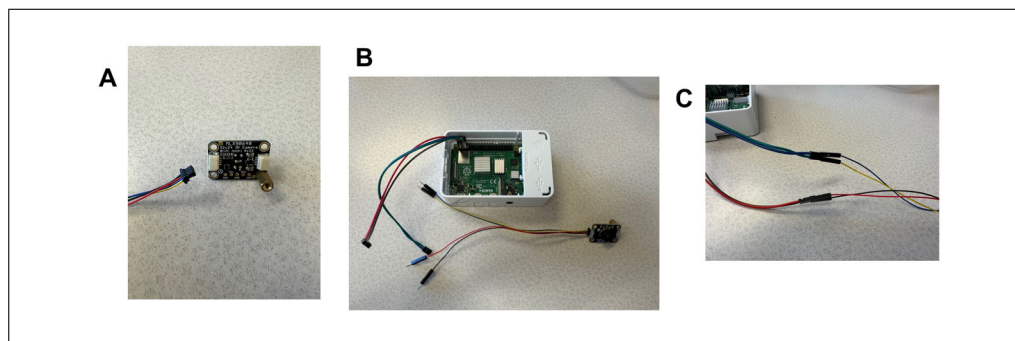


Figure 6 Thermal camera board connection. (A) STEMMA QT / Qwiic JST SH 4-pin cable connected to (B) the Adafruit MLX90640 thermal camera, (C) with jumper wires linked to corresponding colors.

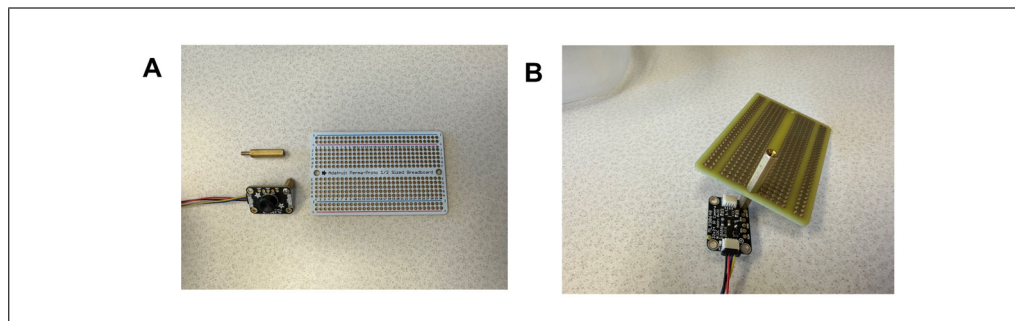


Figure 7 PCB assembly. (A) Thermal camera, breadboard, and brass standoff. (B) Adafruit MLX90640 thermal camera mounted onto the Adafruit Perma-Proto Half-sized Breadboard PCB using a brass standoff.

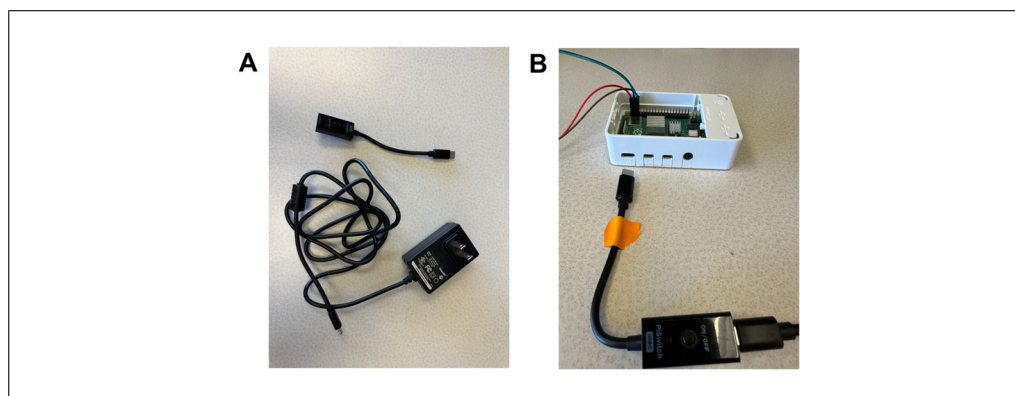


Figure 8 Power supply setup. (A) Power supply equipment and (B) CanaKit Raspberry Pi 4 PiSwitch with connection to the power supply and Raspberry Pi. The red indicator light is visible when properly connected.

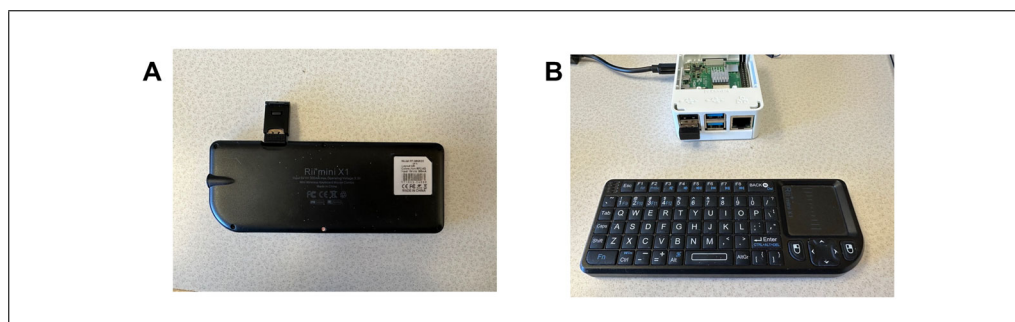


Figure 9 Wireless keyboard connection. (A) USB dongle from the Mini Wireless Keyboard X1 (B) inserted into an available USB port on the Raspberry Pi 4.

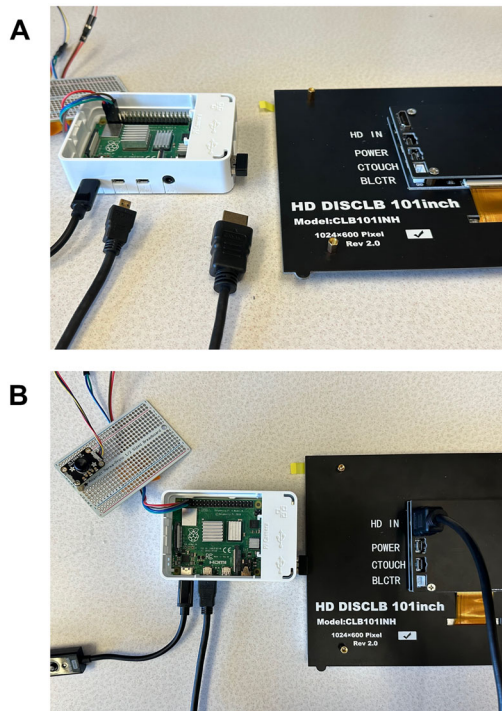


Figure 10 Display connection. (A) Micro HDMI to HDMI cable connecting the Raspberry Pi 4 to (B) the 10.1-in. LCD touch screen display.

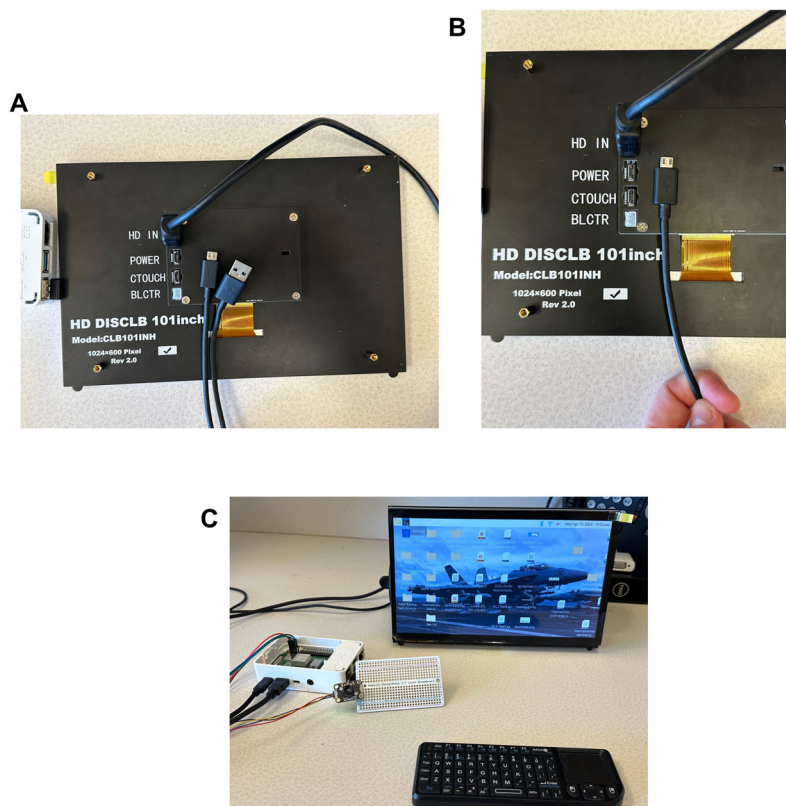


Figure 11 Display power connection. (A) USB-A to Micro-USB cable (B) connecting the touch screen display to a power source, (C) with the screen powered on.

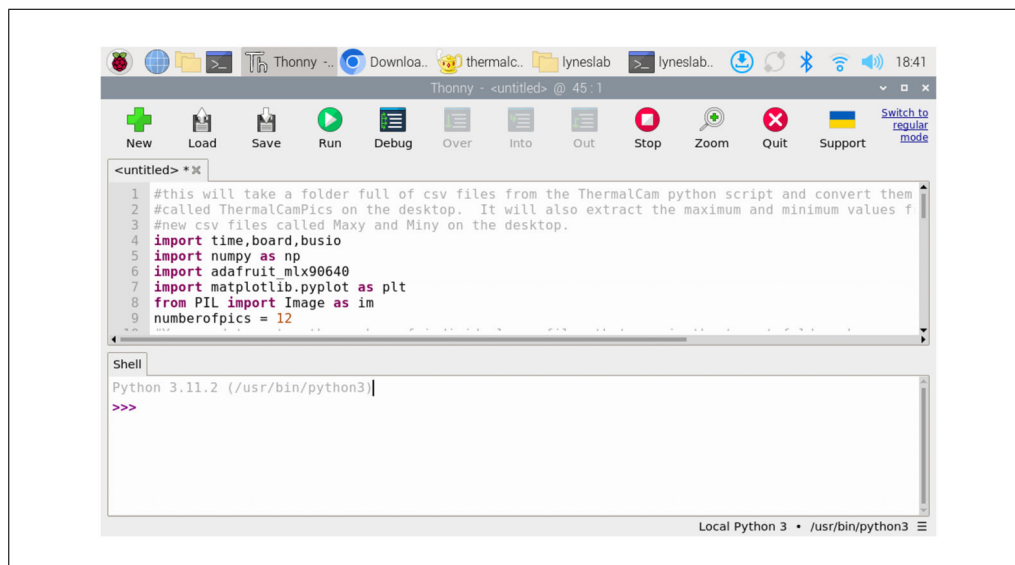


Figure 12 Thonny Python application. The Thonny Python application is shown with code up-loaded.

13. Use the terminal to edit the config file by entering the following command:
 - “sudo nano /boot/config.txt”
14. After the config file opens in the terminal, scroll down to the following line:
 - #dtparam = i2c_arm = on

Change to the following (the text may change from blue to gray when the “#” is deleted):

 - “dtparam = i2c_arm = on,i2c_arm_baudrate = 1000000”

Exit the boot file (ctrl-X) and, when prompted, press “yes” to save the changes made to the config file.
15. Open the terminal and then reboot the computer by entering the following command:
 - “sudo reboot.”
16. Open the terminal and then install the following libraries by entering these commands:
 - “sudo pip3 install RPI.GPIO adafruit-blinka”
 - “sudo pip3 install adafruit-circuitpython-mlx90640”
17. Open the terminal and then reboot the computer by entering the following command:
 - “sudo reboot”
18. Open the Thonny Python editor from the application menu (Annamaa, 2015) (Fig. 12).
19. Open the imaging script for imaging or the analysis script to extract data.

See <https://github.com/mdlynnes/ThermalCam>.

IN VIVO MEASUREMENT OF MOUSE TEMPERATURE AT DIFFERENT AMBIENT CONDITIONS

This protocol describes thermal imaging of mice housed in a diurnal incubator with multiple racks. The mice are kept on a 12-hr light cycle that is synchronized to the standard vivarium schedule, with integrated lights regulated by timers. Although non-invasive,

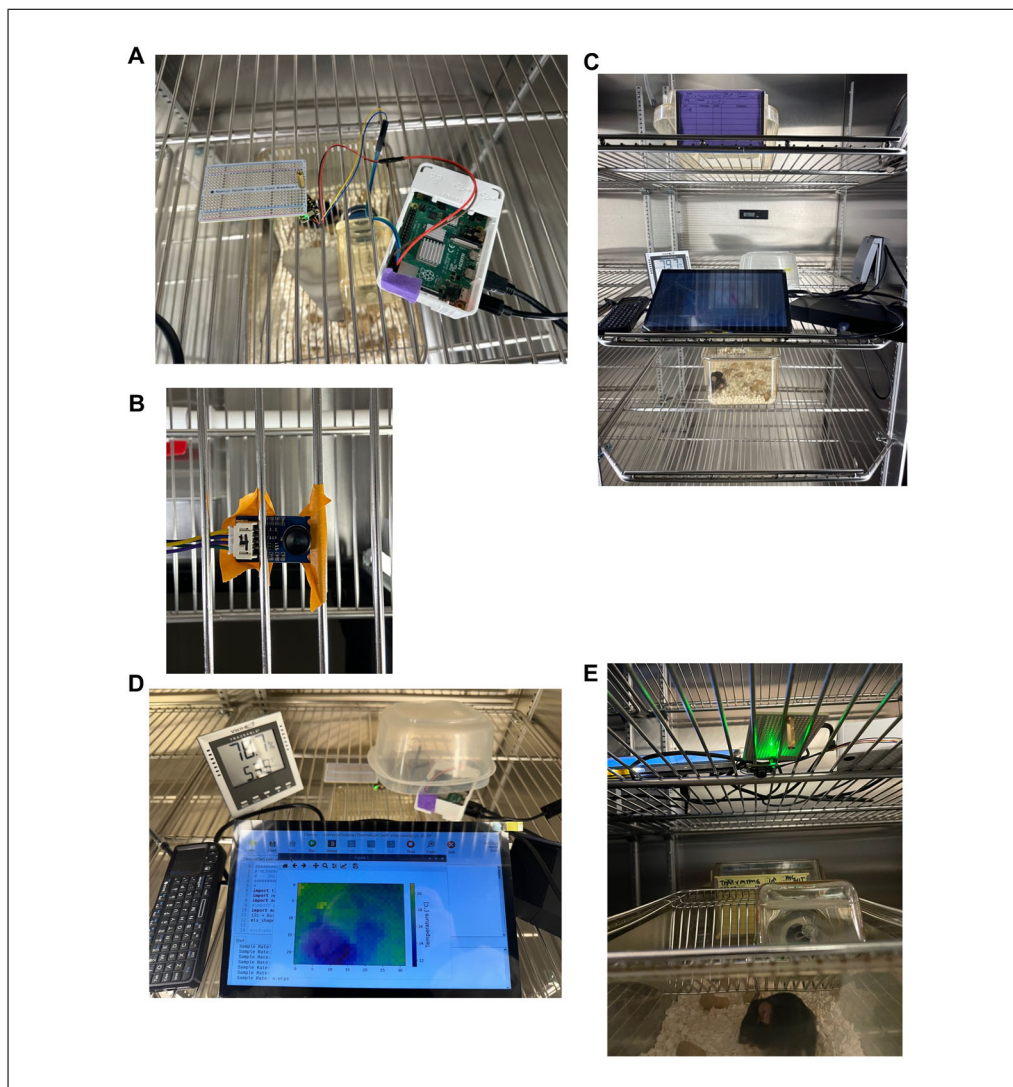


Figure 13 Thermal imaging applications in a diurnal incubator. **(A)** Overhead view of the Raspberry Pi and thermal camera attached to the breadboard, facing downward over the top of the mouse cage in the diurnal incubator. **(B)** View from below of the thermal camera taped to the rack for better support. **(C)** Thermal camera connection to the 10.1-in. LCD Raspberry Pi 4 Model B touch screen. **(D)** View of code running in Thonny Python on the touch screen and the heat map it creates. Once the camera has a second to focus, the heat map will be all blue except a moving tiny circle, which is the mouse in the cage. **(E)** Thermal camera placement above the mouse cage. The breadboard is used to stabilize the camera on the rack above the mouse cage to allow a stable thermal camera reading.

this *in vivo* animal protocol usually must be pre-approved by the local Institutional Animal Care and Use Committee (IACUC). Typically, cages and bedding are changed once a week and monitored daily. Individual mice are housed in each cage, mouse chow is placed on the cage bottom so as not to interfere with the thermal camera, and water is provided by a bottle on top of the cage that is also out of the camera's field of view.

The setup of this thermal imaging system in the diurnal incubator (Fig. 13) takes ~15 min. Imaging of animals using the protocol described here was done in a diurnal incubator over a 24-hr cold exposure test, with 4 hr of acclimation at room temperature followed by cold challenge at 6°C. In particular, each mouse was acclimated to room temperature outside of the incubator and then placed into the incubator once it hit 6°C. Data collection occurred over the course of the experiment, and data were analyzed at the conclusion. The Raspberry Pi thermal camera system (Basic Protocol 1) has been used in

our laboratory to record temperatures of mice in different environmental settings, from room temperature (19°C) to cold challenge at 6°C, for extended periods.

Materials

Mice

Diurnal incubator (Caron Products & Services)

Thermal camera (see Basic Protocol 1)

Mouse cages (with shavings, water bottle, and food)

Microsoft Excel

1. Plug in the diurnal incubator to 120 V power and set temperature to 19°C. Using the thermal camera assembled in Basic Protocol 1, plug in all the power cords for all imaging equipment into a power supply.

It will take ~10 min to reach the desired temperature.

It is convenient to use a multi-outlet extension cable with sufficient amperage capacity (available from Amazon) for these connections.

2. Place a mouse cage containing a mouse on a rack in the incubator and place thermal camera above the cage so that it is facing downward to have an aerial view of the cage (Fig. 13A).

In our studies, mice are kept in the MaineHealth Institute of Research Vivarium. Bedding, food, and water are changed once a week, and daily monitoring is performed.

We only house one mouse per cage to get the most accurate reading for the mouse temperature.

We place the cage inside the thermal incubator because this allows us to control the temperature to which the mouse is exposed. The incubator we use has metal rack shelving, and the thermal camera is placed on the shelf immediately above the cage; this separation prevents the mouse from doing damage to the thermal camera. We have found that taping the camera to a rack within the incubator helps hold the camera secure (Fig. 13B).

3. Open Thonny software on the touch screen (Fig. 13C).

Make sure there is an empty folder entitled “thermal camera” on the desktop for the files to save to; otherwise, the code will not work.

We have found that putting the Raspberry Pi computer within the incubator allows better connection compared to using a longer cord and having the computer outside the incubator. We place a plastic Tupperware container over the Raspberry Pi computer to prevent condensation that could accumulate on the computer when inside the incubator.

4. Remove the cage cover and place food on the cage bottom so as not to interfere with the thermal camera.

Mouse chow is placed on the cage floor to enable a full field of view for the camera.

We use a cage with the following dimensions: 12.5-cm height, 16-cm width, and 64-cm length. When the thermal camera is placed between 5 and 15 cm above the cage, this cage size fits in the field of view of the camera, leaving very little area outside the camera’s field of view; the only area of the cage that is excluded from the thermal camera’s view is under the water bottle. At these distances, the resolution of the camera will allow a single animal to be captured in one pixel, although we have not rigorously tested differences in resolution at different distances.

5. Press “play” on the touch screen (in the top right corner of the program) to initiate recording.

The thermal camera will begin recording, and data are collected every half second. Wait until the “Figure 1” file appears on the computer screen to ensure the camera is properly recording. Changes in color indicating temperature differences within the surface

covered by the figure will indicate that the camera is functioning (Fig. 13D). At this point, the screen can be unplugged and removed from the incubator if desired (Fig. 13E).

6. Check the initial temperature and humidity in the incubator with a digital or gauge thermometer and then set the desired environmental temperature.

The humidity should be 70%.

In our experiments, we typically set an environmental temperature of 20°C (68°F) and let the incubator reach that temperature while setting up the thermal camera. At that point, the temperature can be changed for the experiment; for example, we have tested mice at a thermal temperature of 6°C.

7. To end the recording, click the “Stop” button (in the top right corner of screen).

After the “Stop” button is pressed, all data are saved automatically as a series of comma delimited value files that can be opened using Microsoft Excel.

8. Using the Python data assembler script, extract the maximum value from each .csv file and save the data to a new .csv file called “Max.csv.” Similarly, extract a list of minimum values from each image into a file called “Min.csv.”

These values represent the maximum mouse surface temperature over the course of the experiment and the minimum ambient temperature.

9. Filter the data in Microsoft Excel.

In our experiments, we have found that visual obstruction does not occur very often, but when it does, we account for that in our data analysis by filtering the data. We also filter the data for momentary noise in the data due to hardware faults when the camera takes each measurement. To analyze the data, we initially filter the maximum points to remove any outlier data points. We normally use a maximum of 40°C and filter all datapoints above this temperature because mouse body temperature does not typically increase above 40°C during cold challenge (Hankenson et al., 2018). Using Microsoft Excel software, we use the formula = IF (“temperature value” < 40, “temperature value”, 40) to truncate the data above 40°C. For a typical experiment, we filter out <1% of data points. “Temperature value” is the first data point within the column of all maximum temperature data points. This equation is then propagated in the spreadsheet to evaluate all data points, and a new column is generated where all points that remain to be analyzed are <40. Similarly, we remove all data <0 from the list of minimum temperatures.

10. Plot the surface temperature versus time in a line graph.

COMMENTARY

Understanding Results

In the prototypical data presented here (Fig. 14), male C57BL/6J mice ~8 months of age were exposed to different temperature settings in the incubator (Fig. 14A). In the first dataset, the temperature of the incubator was set to 23°C. Once the incubator reached 23°C, a mouse that had been held at room temperature was placed inside the incubator with its cage over off, leaving just the metal rack holding the water bottle. Mouse chow was placed on top of the bedding on the bottom of the cage. The thermal camera was placed on the shelf above the cage, facing the cage below. To begin the cold challenge, the incubator temperature was decreased to 6°C, recording commenced, and thermal imaging was then conducted for 22 hr. To test the dynamic response to gradual re-

warming, we then raised the temperature to 8°C and continued monitoring. In our second experiment, the incubator temperature was set to 2°C, and the mice were acclimated to this temperature, after which we raised the temperature to 6°C and began recording (Fig. 14B). To test the dynamic response to gradual re-warming, we then raised the temperature to 10°C.

Certain pharmaceuticals can significantly alter body temperature by affecting the body’s thermoregulatory mechanisms (Table 2). Medications such as antipsychotics, diuretics, beta-blockers, stimulants, antihypertensives, and anticholinergic drugs can interfere with the body’s ability to perceive and respond to heat, increasing the risk of heat-related illnesses. Antipsychotics and neuroleptics, for

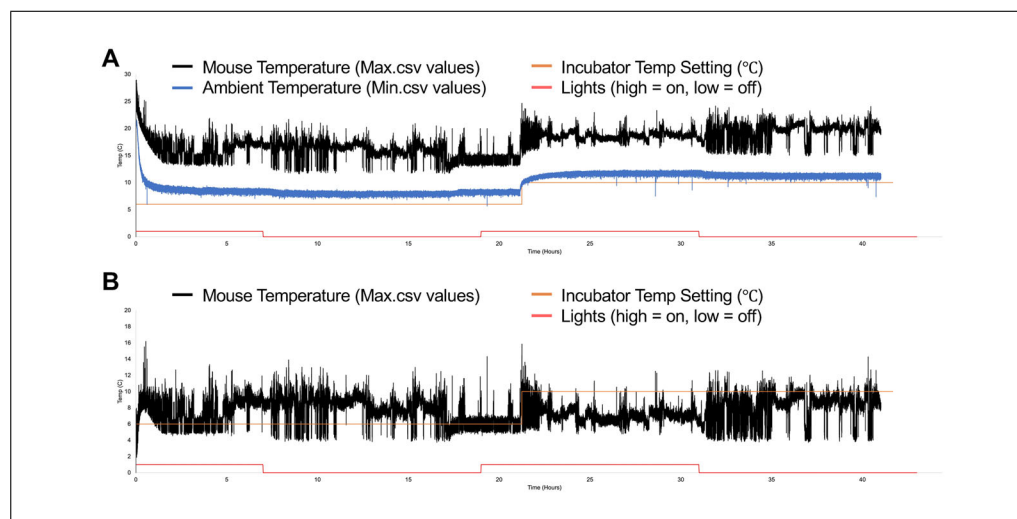


Figure 14 Mouse data from the diurnal incubator. **(A)** A mouse was placed in the incubator, and the temperature setting was increased from 23°C to 6°C. After 31 hr, the temperature was raised to 9°C. The blue line represents the incubator temperature reading from the thermal camera, the orange is the incubator temperature setting, and the red represents the light schedule for the mice. The black lines represent the mouse's change in temperature over the 40 hr. **(B)** The experiment in (A) was repeated, except the mouse was baselined at 2°C and then the temperature was raised to 6°C, and after 21 hr, it was raised to 10°C.

Table 2 Effects of Pharmaceuticals on Metabolic Activity

Category of drug	Examples of drug	Use and effect ^a
Anti-obesity drugs	Orlistat, liraglutide, phentermine	Work by reducing appetite, increasing satiety, or inhibiting the absorption of dietary fat, ultimately leading to a reduction in caloric intake and metabolic activity
Thyroid medications	Levothyroxine, liothyronine	Used to treat hypothyroidism and can increase metabolic activity by regulating thyroid hormone levels, which play a crucial role in metabolism
Anti-diabetic drugs	Metformin, thiazolidinediones	Can improve insulin sensitivity and glucose metabolism, indirectly affecting metabolic activity
Beta-blockers	Propranolol, metoprolol	Commonly used to treat hypertension and certain cardiovascular conditions, can reduce metabolic activity by decreasing heart rate and cardiac output
Stimulants	Amphetamines, ADHD medications	Can increase metabolic activity by stimulating the central nervous system and increasing energy expenditure
Corticosteroids	Prednisone, cortisone	These anti-inflammatory drugs can have metabolic effects, including increased glucose production, protein breakdown, and altered lipid metabolism
Antidepressants	Fluoxetine, sertraline	Can affect appetite and metabolic activity as a side effect

^a Comparison of different categories of drugs with effects on metabolic activity. Pharmaceuticals' effects on metabolic activity can vary depending on the specific drug, dosage, and individual patient characteristics. Monitoring metabolic activity can be valuable in assessing the efficacy and potential side effects of these medications.

instance, can lead to heat sensitivity and disrupt the body's cooling processes by blocking dopamine and acetylcholine receptors, which are crucial for thermoregulation. Stimulants used for attention-deficit hyperactivity disorder (ADHD), such as methylphenidate and dexamfetamine, raise body temperature by

acting on the hypothalamus. Additionally, the use of TRPV1 antagonists, like AMG517, has been shown to induce hyperthermia in both animal models and human clinical trials (Yue et al., 2022). These medications can either increase body temperature directly or impair the body's ability to dissipate heat, making

Table 3 Toxicants’ Impact on Metabolic Activity

Toxicant	Effect on metabolic activity ^a
Persistent organic pollutants (POPs)	Compounds like polychlorinated biphenyls (PCBs), dioxins, and certain pesticides can disrupt metabolic processes, leading to alterations in energy expenditure, lipid metabolism, and glucose homeostasis.
Heavy metals	Exposure to heavy metals like lead, cadmium, and mercury can interfere with various metabolic pathways, including energy production, enzyme function, and oxidative stress.
Air pollutants	Particulate matter and other air pollutants have been linked to metabolic disorders, such as insulin resistance and obesity, potentially through mechanisms involving inflammation and oxidative stress.
Endocrine-disrupting chemicals (EDCs)	Substances like bisphenol A (BPA), phthalates, and certain pesticides can interfere with hormone signaling pathways, which can indirectly affect metabolic processes.
Mycotoxins	Toxic secondary metabolites produced by certain fungi, such as aflatoxins and ochratoxins, can disrupt metabolic processes and contribute to metabolic disorders like fatty liver disease.
Alcohol and drugs of abuse	Excessive alcohol consumption and the use of certain recreational drugs can have profound effects on metabolic activity, leading to alterations in energy balance, lipid metabolism, and glucose regulation.

^a Different toxicants’ effects on metabolic activity. The impact of toxicants on metabolic activity can vary depending on the specific compound, the dose, and the duration of exposure. Understanding the effects of these toxicants on metabolic processes is crucial for assessing their potential health risks and developing appropriate interventions or preventive measures.

individuals more susceptible to heat stress, especially during extreme weather conditions. In Figure 14A, the animal appropriately regulates body temperature as a function of cold stress, decreasing body temperature during the initial acclimatization to cold and increasing body temperature when the incubator temperature is increased. Animals with hyperthermia show a delayed or decreased reduction in body temperature in response to cold challenge.

Toxicants can also significantly impact body temperature regulation, leading to both hyperthermia and hypothermia, depending on the specific substance and exposure conditions (Table 3). Many poisons and toxic chemicals have been shown to disrupt the body’s thermoregulatory system, causing abnormal fluctuations in core temperature. For example, certain organophosphate pesticides like chlorpyrifos can induce an initial hypothermic response followed by a prolonged elevation in body temperature (Wang & Steinberg, 2022). Other toxicants, such as atropine and pentachlorophenol, are known to cause hyperthermia, whereas substances like ethanol can lead to hypothermia. The mechanisms behind these temperature alterations vary, but they often involve disruption of metabolic processes, interference with the central nervous system’s thermoregulatory centers, or activation of inflammatory pathways. In

Figure 14A, toxicants that induce hypothermia would show a decreased body temperature that was exacerbated by cold challenge. Additionally, environmental factors like heat stress can exacerbate the effects of toxicants on body temperature, potentially increasing their harmful impacts. Understanding these interactions is crucial for accurately assessing toxicity and developing appropriate safety measures, as changes in body temperature can significantly influence the metabolism and distribution of drugs and toxicants in the body.

Concluding Remarks

The application of IRT in mouse metabolic research is based on the principle that all objects with a temperature above absolute zero emit infrared radiation. The intensity of this radiation is directly proportional to the object’s temperature, allowing for accurate temperature measurements without physical contact. This non-invasive quality is particularly advantageous when working with small, stress-sensitive animals like mice (Watanabe, 2023). IRT has emerged as a powerful and non-invasive tool for studying metabolism and thermoregulation in mice. By utilizing a low-cost FLIR camera, researchers can gain valuable insights into various aspects of mouse physiology without causing undue stress or interfering with natural behaviors. This technology offers a unique opportunity to observe and

quantify thermal changes in real time, providing a window into the metabolic processes occurring within the animal's body.

Acknowledgments

M.D.L. is a project lead on grants from the U.S. National Institutes of Health (NIH P20GM121301, P20GM139768, and P20GM139745).

Author Contributions

Breanna Page: Investigation; methodology; writing—original draft; writing—review and editing. **Carolina Cora:** Investigation; methodology; writing—original draft; writing—review and editing. **James Reilly:** Methodology; software; writing—review and editing. **Ryan Reno:** Methodology; writing—review and editing. **Wadak Harbi:** Investigation; methodology; writing—review and editing. **Maureen S. Lynes:** Writing—original draft; writing—review and editing. **Michael A. Lynes:** Conceptualization; writing—original draft; writing—review and editing. **Matthew D. Lynes:** Conceptualization; data curation; funding acquisition; investigation; methodology; software; supervision; writing—original draft; writing—review and editing.

Conflict of Interest

The authors declare no conflict of interest.

Data Availability Statement

All datasets generated for this study are included in this article.

Code Availability Statement

The code described in this article is freely available at <https://github.com/mdlynes/ThermalCam>.

Literature Cited

- Annamaa, A. (2015). Thonny: A Python IDE for learning programming. In *Proceedings of the 2015 ACM Conference on Innovation and Technology in Computer Science Education* (p. 343). <https://doi.org/10.1145/2729094.2754849>
- Bagavathiappan, S., Saravanan, T., Philip, J., Jayakumar, T., Raj, B., Karunanithi, R., Panicker, T. M., Korath, M. P., & Jagadeesan, K. (2009). Infrared thermal imaging for detection of peripheral vascular disorders. *Journal of Medical Physics*, 34(1), 43–47. <https://doi.org/10.4103/0971-6203.48720>
- Blessing, W. W. (2018). Thermoregulation and the ultradian basic rest-activity cycle. *Handbook of Clinical Neurology*, 156, 367–375. <https://doi.org/10.1016/b978-0-444-63912-7.00022-9>
- Chouchani, E. T., Kazak, L., & Spiegelman, B. M. (2019). New advances in adaptive thermogenesis: UCPI and beyond. *Cell Metabolism*, 29(1), 27–37. <https://doi.org/10.1016/j.cmet.2018.11.002>
- Coskun, A., Zarepour, A., & Zarrabi, A. (2023). Physiological rhythms and biological variation of biomolecules: The road to personalized laboratory medicine. *International Journal of Molecular Sciences*, 24(7), 6275. <https://doi.org/10.3390/ijms24076275>
- Cypess, A. M., Lehman, S., Williams, G., Tal, I., Rodman, D., Goldfine, A. B., Kuo, F. C., Palmer, E. L., Tseng, Y. H., Doria, A., Kolodny, G. M., & Kahn, C. R. (2009). Identification and importance of brown adipose tissue in adult humans. *The New England Journal of Medicine*, 360(15), 1509–1517. <https://doi.org/10.1056/NEJMoa0810780>
- Cypess, A. M., White, A. P., Vernochet, C., Schulz, T. J., Xue, R., Sass, C. A., Huang, T. L., Roberts-Toler, C., Weiner, L. S., Sze, C., Chacko, A. T., Deschamps, L. N., Herder, L. M., Truchan, N., Glasgow, A. L., Holman, A. R., Gavrila, A., Hasselgren, P. O., Mori, M. A., ... Tseng, Y. H. (2013). Anatomical localization, gene expression profiling and functional characterization of adult human neck brown fat. *Nature Medicine*, 19(5), 635–639. <https://doi.org/10.1038/nm.3112>
- Frontini, A., & Cinti, S. (2010). Distribution and development of brown adipocytes in the murine and human adipose organ. *Cell Metabolism*, 11(4), 253–256. <https://doi.org/10.1016/j.cmet.2010.03.004>
- Hankenson, F. C., Marx, J. O., Gordon, C. J., & David, J. M. (2018). Effects of rodent thermoregulation on animal models in the research environment. *Comparative Medicine*, 68(6), 425–438. <https://doi.org/10.30802/aalascm-18-000049>
- Holstila, M., Pesola, M., Saari, T., Koskensalo, K., Raiko, J., Borra, R. J., Nuutila, P., Parkkola, R., & Virtanen, K. A. (2017). MR signal-fat-fraction analysis and T2* weighted imaging measure BAT reliably on humans without cold exposure. *Metabolism*, 70, 23–30. <https://doi.org/10.1016/j.metabol.2017.02.001>
- Hrisko, J. (2020). High resolution thermal camera with Raspberry Pi and MLX90640. Retrieved from <https://makersportal.com/blog/2020/6/8/high-resolution-thermal-camera-with-raspberry-pi-and-mlx90640>
- Kuroyanagi, A., Ukyo, R., Kodama, Y., Eto, T., Okubo, Y., Kobayashi, I., Seiji, I., Tetsuo, M., & Sakamoto, S. H. (2022). Body temperature measurement reveals the reproductive profile of female *Apodemus speciosus* under laboratory and field conditions. *Mammal Study*, 47(3), 1–11. <https://doi.org/10.3106/ms2021-0048>
- Lidell, M. E., Betz, M. J., Dahlqvist Leinhard, O., Heglind, M., Elander, L., Slawik, M., Mussack, T., Nilsson, D., Romu, T., Nuutila, P., Virtanen, K. A., Beuschlein, F., Persson, A., Borga, M., & Enerbäck, S. (2013). Evidence for two types of brown adipose tissue in humans. *Nature Medicine*, 19(5), 631–634. <https://doi.org/10.1038/nm.3017>

- Madhupathy, S. R., Bury, M. I., Wang, L. W., Ciatti, J. L., Avila, R., Huang, Y., Sharma, A. K., & Rogers, J. A. (2024). Miniaturized implantable temperature sensors for the long-term monitoring of chronic intestinal inflammation. *Nature Biomedical Engineering*, 8(8), 1040–1052. <https://doi.org/10.1038/s41551-024-01183-w>
- Mo, Q., Salley, J., Roshan, T., Baer, L. A., May, F. J., Jaehnig, E. J., Lehnig, A. C., Guo, X., Tong, Q., Nuotio-Antar, A. M., Shamsi, F., Tseng, Y. H., Stanford, K. I., & Chen, M. H. (2017). Identification and characterization of a supraclavicular brown adipose tissue in mice. *JCI Insight*, 2(11), e93166. <https://doi.org/10.1172/jci.insight.93166>
- Monshipouri, M., Aliahmad, B., Ogrin, R., Elder, K., Anderson, J., Polus, B., & Kumar, D. (2021). Thermal imaging potential and limitations to predict healing of venous leg ulcers. *Scientific Reports*, 11(1), 13239. <https://doi.org/10.1038/s41598-021-92828-2>
- Ootsuka, Y., de Menezes, R. C., Zaretsky, D. V., Alimoradian, A., Hunt, J., Stefanidis, A., Oldfield, B. J., & Blessing, W. W. (2009). Brown adipose tissue thermogenesis heats brain and body as part of the brain-coordinated ultradian basic rest-activity cycle. *Neuroscience*, 164(2), 849–861. <https://doi.org/10.1016/j.neuroscience.2009.08.013>
- Ramirez-GarciaLuna, J. L., Rangel-Berridi, K., Bartlett, R., Fraser, R. D., & Martinez-Jimenez, M. A. (2022). Use of infrared thermal imaging for assessing acute inflammatory changes: A case series. *Cureus*, 14(9), e28980. <https://doi.org/10.7759/cureus.28980>
- Roberts, S. B., Coward, W. A., Schlingenseipen, K. H., Nohria, V., & Lucas, A. (1986). Comparison of the doubly labeled water (2H2(18)O) method with indirect calorimetry and a nutrient-balance study for simultaneous determination of energy expenditure, water intake, and metabolizable energy intake in preterm infants. *American Journal of Clinical Nutrition*, 44(3), 315–322. <https://doi.org/10.1093/ajcn/44.3.315>
- Rubio, W. B., Cortopassi, M. D., & Banks, A. S. (2023). Indirect calorimetry to assess energy balance in mice: Measurement and data analysis. *Methods in Molecular Biology*, 2662, 103–115. https://doi.org/10.1007/978-1-0716-3167-6_9
- Sacks, H., & Symonds, M. E. (2013). Anatomical locations of human brown adipose tissue: Functional relevance and implications in obesity and type 2 diabetes. *Diabetes*, 62(6), 1783–1790. <https://doi.org/10.2337/db12-1430>
- Shimatani, H., Inoue, Y., Maekawa, Y., Miyake, T., Yamaguchi, Y., & Doi, M. (2021). Thermographic imaging of mouse across circadian time reveals body surface temperature elevation associated with non-locomotor body movements. *PLoS One*, 16(5), e0252447. <https://doi.org/10.1371/journal.pone.0252447>
- Smarr, B., & Kriegsfeld, L. J. (2022). Female mice exhibit less overall variance, with a higher proportion of structured variance, than males at multiple timescales of continuous body temperature and locomotive activity records. *Biology of Sex Differences*, 13(1), 41. <https://doi.org/10.1186/s13293-022-00451-1>
- Tseng, Y. H., Cypess, A. M., & Kahn, C. R. (2010). Cellular bioenergetics as a target for obesity therapy. *Nature Reviews Drug Discovery*, 9(6), 465–482. <https://doi.org/10.1038/nrd3138>
- Virtanen, K. A. (2016). The rediscovery of BAT in adult humans using imaging. *Best Practice & Research: Clinical Endocrinology & Metabolism*, 30(4), 471–477. <https://doi.org/10.1016/j.beem.2016.09.001>
- Wang, B., & Steinberg, G. R. (2022). Environmental toxicants, brown adipose tissue, and potential links to obesity and metabolic disease. *Current Opinion in Pharmacology*, 67, 102314. <https://doi.org/10.1016/j.coph.2022.102314>
- Watanabe, S. (2023). Infrared thermography for non-invasive measurement of social inequality aversion in rodents and potential usefulness for future animal-friendly studies. *Frontiers in Behavioral Neuroscience*, 17, 1131427. <https://doi.org/10.3389/fnbeh.2023.1131427>
- Yue, W. W. S., Yuan, L., Braz, J. M., Basbaum, A. I., & Julius, D. (2022). TRPV1 drugs alter core body temperature via central projections of primary afferent sensory neurons. *eLife*, 11, e80139. <https://doi.org/10.7554/eLife.80139>